Communication

A Triband Low-Profile High-Gain Planar Antenna Using Fabry–Perot Cavity

Fan Qin, Steven Gao, Qi Luo, Gao Wei, Jiadong Xu, Jianzhou Li, Changying Wu, Chao Gu, and Chunxu Mao

***Abstract*— A triband antenna with high gain and low profile is proposed. This antenna is based on the concept of Fabry–Perot cavity antenna (FPCA) and three resonances are obtained by employing two frequency selective surface (FSS) layers. Two FSS layers lead to two resonant frequencies by making each FSS layer satisfy the resonant condition of Fabry–Perot cavity. The third resonant frequency is obtained by exploiting the combined effects of the two FSS layers together. The operating principle of this proposed antenna is explained and the achievable frequency range is investigated. It is shown that the proposed method enables all three resonant frequencies to be independently tuned within certain frequency range. Because of the 0° reflection phase of the combined-FSSs, the present antenna has a low profile. To verify the design concept, one C-/X-/Ku-band FPCA is designed, fabricated and tested. Experimental results agree well with the simulated results. High gain with good impedance matching in three bands is obtained, which reaches a peak gain of 13.4 dBi at 5.2 GHz, 18.9 dBi at 9.7 GHz, and 20 dBi at 14.6 GHz. The overall height of the proposed antenna is approximately 0.36 wavelength at its lowest operating frequency.**

***Index Terms*— Antenna, array, fabry–Perot, high gain, partially reflective surface, triband.**

I. Introduction

The high gain antennas and array antennas that operate over multiple frequency bands are of significant interest to wireless industries, due to the need of satisfying the requirements of various wireless systems at different frequency bands such as synthetic aperture radars, satellite communications Global Navigation Satellite Systems, terrestrial mobile communications and deep-space links [1]. Several techniques have been used to realize multiband antennas including multipatch microstrip structure, stacked microstrip antenna, and multiband slot antenna. Classical high gain antennas such as large reflectors [2], waveguide horns [3], dielectrics lenses [4], and large-scale antenna arrays [5] offer attractive solutions to achieve high gain performance. However, these techniques have limited applications due to their design complexity, bulky size, high cost, and/or significant power losses in the feed network. Some dual-band high-gain arrays were reported [6], [7] but they have rather complicated structures. Therefore, it is necessary to investigate novel solutions to design multiband high-gain antennas with planar structures, low profile, simple feed mechanisms, and low cost.

Fabry–Perot cavity antenna (FPCA) has been widely investigated in recent years because of its advantages of high gain, easy fabrication, simple feed system, and low cost [8]. An FPCA typically consists of a primary feed antenna located in a resonant cavity formed between a perfect reflector and a partially reflective surface (PRS), which is usually constructed of a dielectric superstrate or a periodic surface. A significant enhancement of antenna's directivity can be achieved using the multiple reflections between the ground plane and the PRS. The operating frequency of the FPCA depends on the following equation [8]:

$$f = \frac{c}{4\pi h}(\varphi_{\text{prs}} + \pi - 2N\pi), N = 0, 1, 2 \ldots \tag{1}$$

where h is the cavity height, φ_{prs} is the reflection phase of the PRS and π is the reflection phase of the ground plane.

The directivity of the FPCA relative to that of the feed antenna can be written as

$$D_r = 10 \log \frac{1+\Gamma}{1-\Gamma} \tag{2}$$

where D_r is the relative directivity and Γ is the reflection magnitude of the PRS.

Various dual-band FPCAs have been implemented so far. A method employing the electro-magnetic bandgap materials in the FPCAs was reported to achieve dual-band operation [9]. The dual-band FPCAs based on inverted reflection phase gradient of the PRS were achieved in [10] and [11], where a single layer PRS with slot and two dielectric slabs were applied to obtain two different resonances, respectively. In [12], a dual-frequency FPCA was discussed by utilizing the first and second order resonances of the resonant cavity. One limitation of these dual-band FPCAs is that it is difficult to design two frequencies independently. In [13], two orthogonal dipole arrays printed on two substrates as the PRS were employed to form two separate resonate cavities for dual-band FPCA. More recently, a simpler configuration was reported in [14], where a patch with slot printed on a substrate layer was used as the PRS element. However, these dual-band FPCAs cannot support the same polarization as well as circular polarization at two operating frequencies due to the asymmetric configuration of the PRS element. A triband FPCA operating at 10.8, 11.3, and 12.2 GHz was proposed in [15]. However, it is not flexible to design the operating frequencies. Hence there is a need to investigate novel techniques of designing planar triband high-gain antennas with flexible frequency design.

This communication presents our research work on triband high-gain FPCA with low-profile, planar structure, easy fabrication and low cost. The design technique of how to use two frequency selective surface (FSS) layers to obtain three resonant frequencies of the Fabry–Perot resonant cavity is detailed. One advantage of this triband PRS antenna is its flexibility of antenna design in tuning frequency and choosing frequency ratio. Design guidelines on how to tune the operating frequencies independently within the achievable frequency ratio are also presented. Compared to other reported designs on the multiband Fabry–Perot resonant cavity antennas, the proposed antenna has a lower profile with comparable radiation performance.

II. Design Principle and Study of Frequency Range

A. Units of the FSS Layers

Fig. 1(a) and (b) shows the configuration and side view of the triband FPCA, respectively. Two FSS layers are mounted above the ground plane with the cavity heights of h_1 and h_2, which form two separated cavities with the ground plane resonating at f_1 and f_2,

Manuscript received December 23, 2015; revised December 26, 2016; accepted January 1, 2017. Date of publication February 16, 2017; date of current version May 3, 2017.

F. Qin, G. Wei, J. Xu, J. Li, and C. Wu are with the School of Electronics and Information, Northwestern Polytechnical University, Xi'an 710072, China (e-mail: fan.qin@outlook.com).

S. Gao, Q. Luo, C. Gu, and C. Mao are with the School of Engineering and Digital Arts, University of Kent, Canterbury CT2 7NT, U.K.

Color versions of one or more of the figures in this communication are available online at http://ieeexplore.ieee.org.

Digital Object Identifier 10.1109/TAP.2017.2670564

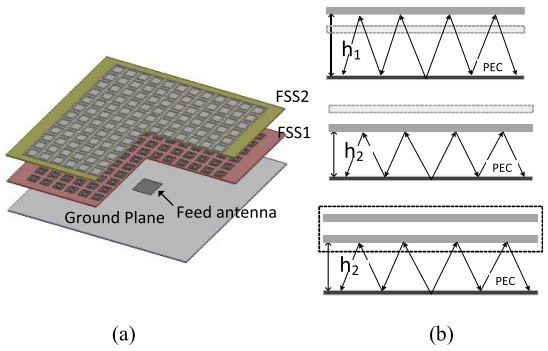

Fig. 1. (a) Basic configuration of the triband PRS antenna. (b) Working principle of the triband PRS antenna.

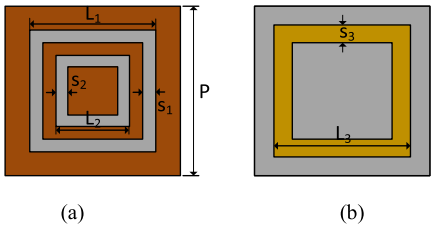

Fig. 2. Units of the two FSS structures. (a) FSS1. (b) FSS2.

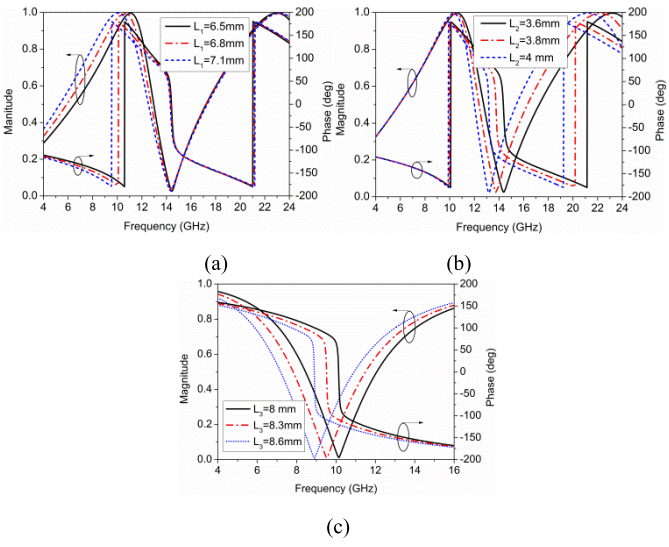

Fig. 3. Reflection coefficients of the two FSSs. (a) FSS1 with different L_1 ($S_1 = S_2 = 0.5$ mm). (b) FSS1 with different L_2($S_1 = S_2 = 0.5$ mm). (c) FSS2 with different L_3($S_3 = 1$ mm).

respectively. The FSS layers are required to have sufficient reflection magnitude at one frequency and be transparent at the other frequencies. The third frequency (f_3) is achieved by combining the two FSSs together to produce another resonance.

The structures of the two FSS layers shown in Fig. 2 are considered. The FSS units are printed on 0.8 mm Rogers 4003C substrate with $\varepsilon_r = 3.55$. FSS1 consists of two metallic rings. The length of the outer ring is set as L_1 and the inner one is L_2 with the width of S_1 and S_2, respectively. The FSS2 is a ring slot with the length of L_3 and the width of S_1. Both of these two structures have the same periodicity P.

Full-wave simulations (CTS MWS) with the consideration of periodic boundary are employed to study the reflection coefficient of each FSS. The calculated reflection coefficient with different parameters is shown in Fig. 3. It can be seen in Fig. 3(a) and (b)

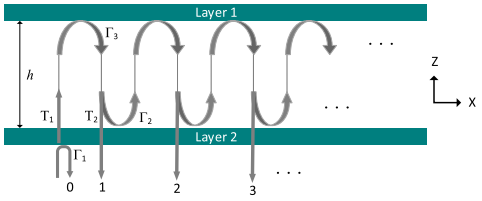

Fig. 4. Ray-model of the combined-FSSs.

that the FSS1 has the bandpass characteristics in *Ku*-band. There are two frequencies having a full reflection in FSS1, which is determined by L_1 and L_2, respectively. The bandpass frequency occurs between the two full-reflection frequencies. Varying L_1 and L_2 can adjust the bandwidth and the frequency of the bandpass, respectively. The properties of bandpass in FSS2 is determined by L_3. The bandpass frequency moves to lower frequency with the increase of the L_3. Based on the performance of these two FSS layers, a dual-band FPCA operating in *X*- and *Ku*-bands can be achieved.

B. Study of the Third Resonance

The third frequency (f_3) is produced by combining the two FSS layers together. The ray optics analysis can be used to study the reflection response of the combined-FSS layers. With reference to Fig. 4, considering a plane wave incident on the combined-FSSs from the bottom of the layer 2, where R_0, R_1, R_2, etc., are the reflection coefficient associated with each of the numbered partial rays reflected by the combined-FSSs. They can be expressed as

$$\begin{aligned} R_0 &= \Gamma_1 \\ R_1 &= T_1 T_2 \Gamma_3 e^{-2j\beta h} \\ R_2 &= T_1 T_2 \Gamma_2 \Gamma_3^2 e^{-4j\beta h} \end{aligned} \tag{3}$$

where Γ_1 and Γ_2 are the complex reflection coefficient of the layer 2 illustrated by the plane wave along $+z$ and $-z$ directions, respectively. Γ_3 is the complex reflection of the layer 1 along the + $z$direction. T_1 and T_2 are the transmission coefficient of the layer 2 along $+z$ and $-z$ direction, respectively. h is the air-gap between these two layers.

The total reflection coefficient of the combined-FSSs is obtained as the summation of the reflected rays, which is derived as

$$R = \Gamma_1 + T_1 T_2 \Gamma_3 e^{-2j\beta h} \sum_{n=0}^{\infty} (\Gamma_2 \Gamma_3 e^{-2j\beta h})^n. \tag{4}$$

Since $|\Gamma_2 \Gamma_3| < 1$, (4) can be simplified by exploiting the infinite geometric series identity

$$R = \Gamma_1 + \frac{T_1 T_2 \Gamma_3 e^{-2j\beta h}}{1 - \Gamma_2 \Gamma_3 e^{-2j\beta h}}. \tag{5}$$

The parameters of the FSS1 and FSS2 are set as $L_1 = 6.8$ mm, $L_2 = 3.6$ mm, $L_3 = 8.3$ mm, $S_1 = S_2 = 0.5$ mm and $S_3 = 1$ mm. In this case, $f_1 = 14.5$ GHz and $f_2 = 9.5$ GHz.

There are two options to combine these two FSS layers as shown in Fig. 5. The option 1 is that both of the two cavities work at the first order resonant length ($N = 0$): $h_1 = 9.9$ mm and $h_2 = 16$ mm according to (1). In this case, the FSS1 is mounted on the top of the second FSS [Fig. 5(a)]. The option 2 is that the FSS1 keeps working at the first order resonant while the FSS2 works at the second order resonant, whose cavity height is increased to $h_1 = 20.3$ mm ($N = 1$). In this case, the FSS2 is on the top of the FSS 1[Fig. 5(b)]. It should be noted that with either configuration the FPCA can operate at 14.5 and 9.5 GHz.

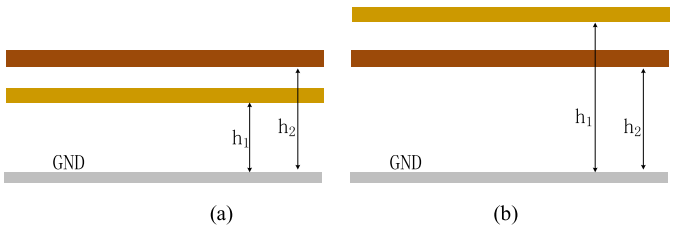

Fig. 5. Two options of combing the two FSS layers. (a) Option 1. (b) Option 2.

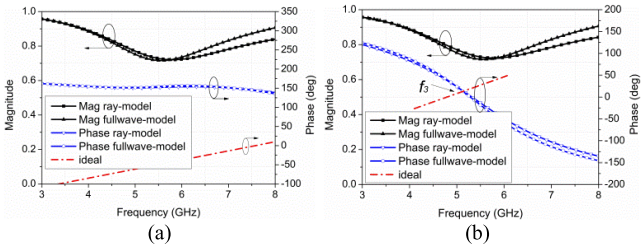

Fig. 6. Reflection coefficients of the combined-FSSs. (a) Option 1. (b) Option 2.

To confirm the third resonant frequency f_3 the phase response of the combined-FSSs and the required reflection phase of the combined-FSSs can be calculated using (5) and (1), respectively. For option 1, the cavity height forming the third resonance is 9.9 mm and for option 2, the cavity height changes to 16 mm. Fig. 6 shows the response of the combined-FSSs calculated by using the both ray optics analysis and full-wave simulation as well as the required reflection phase of the combined-FSSs in order to obtain f_3.

There is a good agreement between the simulated results and those obtained from the ray tracking model. It can be observed that the reflection phase of the option 1 is around 150°, which cannot satisfy the required reflection phase, as shown in Fig. 6(a). For the option 2, the combined-FSSs has the property of artificial magnetic conductors (AMC), where a 0° reflection phase happens at 5.3 GHz and the reflection phase varies from 123° to −145° from 3 to 8 GHz. This combination presents the AMC property in *C*-band because FSS1 and FSS2 show the capacitive and inductive characteristics in *C*-band, respectively, as shown in Fig. 3. When such two FSSs are combined, namely the bottom of the combined-FSSs acts as capacitance and the top of the combined-FSSs acts as inductance, the property of 0° reflection phase can be produced [16]. It can be seen that an intersection happens at 5.2 GHz in Fig. 6(b). Meanwhile, at this frequency the reflection magnitude is high enough. Thus, three resonances occurring in one FPCA is achieved by utilizing the two FSS layers with the configuration of option 2.

C. Achievable Frequency Range and Frequency Ratio

In this section, the operating frequency range and frequency ratio are studied. As will be demonstrated later, although f_3 is related to f_1 and f_2, the frequency ratio can be controlled so the present design approach can be adapted to the design of other triband antennas with different frequency ratios. To better demonstrate this tuning technique, in this communication, the highest resonant frequency is fixed at 14.5 GHz and the height of cavity 1 keeps as 20.3 mm.

To obtain significant enhancement of directivity, Γ is required to be sufficiently large according to (2). Thus, two conditions should be satisfied: one is to have sufficient reflection magnitude to guarantee the directivity enhancement at each operating frequency. In our design, Γ is chosen to be above 0.7. The other condition is that to guarantee the third resonant frequency, the combined-FSSs should be same as the configuration of the option 2, which means the height

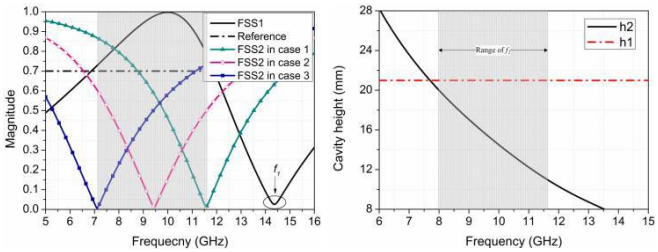

Fig. 7. Frequency range of f_2. (a) Reflection magnitude of the two FSSs. (b) Cavity height versus frequency.

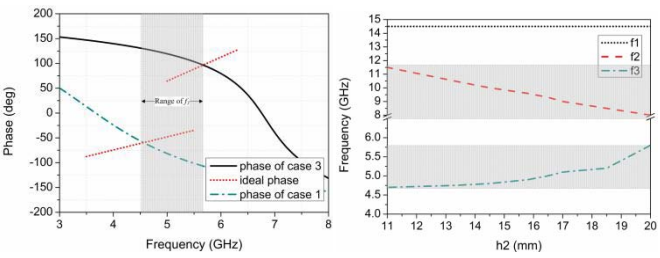

Fig. 8. (a) Frequency ranges of f_3. (b) Working frequency versus h_2.

TABLE I
FREQUENCY RATIO OF THE PROPOSED TRIBAND FPCA

Frequency range (GHz)	f_1/f_2	f_2/f_3	f_1/f_3
14.6 (f_1)			
8-11.5 (f_2)	1.26-1.81	1.40-2.56	2.54-3.22
4.5-5.7 (f_3)			

of cavity 2 needs to be lower than the one of cavity 1. Fig. 7(a) shows that f_2 can be designed from 7 to 11.5 GHz under the first requirement. Within this frequency range, the reflection magnitude is above 0.7 at f_1 and f_2. To guarantee the second condition, the f_2 needs to be higher than 8 GHz, as shown in Fig. 7(b). Thus the frequency range of f_2 can be found from 8 to 11.5 GHz.

The operating frequency of f_3 can be determined according to the frequency range of f_2. The maximum and minimum f_2 are 11.5 and 8 GHz, respectively. The minimum f_3 is found when f_2 works at the maximum frequency (11.5 GHz). Then f_3 increases to 5.7 GHz when f_2 operates at the minimum frequency of 8 GHz, as shown in Fig. 8(a), resulting in the frequency range of f_3 from 4.5 to 5.7 GHz. Fig. 8(b) plots the three operating frequencies versus the height of the cavity 2. The highest frequency keeps unchanged. The f_2 decreases with the increase of h_2, which agrees with (1). The third resonance is determined by the both combined-FSSs and height of the cavity 2. It increases with the decrease of f_2. The curves in Fig. 8(b) offer a guide in the design process since it directly helps the designer to tune the triband FPCA to specified operating frequencies. The frequency ratios are summarized in Table I. As can be seen, this proposed antenna provides a good flexibility of antenna design in choosing frequency ratio.

D. Independently Frequency Tuning of f_3

In this section, a technique to tuning the f_3 independently is discussed. According to (1), the working frequencies, f_1 and f_2,

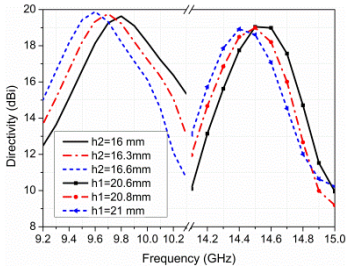

Fig. 9. Directivity of the FPCA with different cavity heights in X- and Ku-bands.

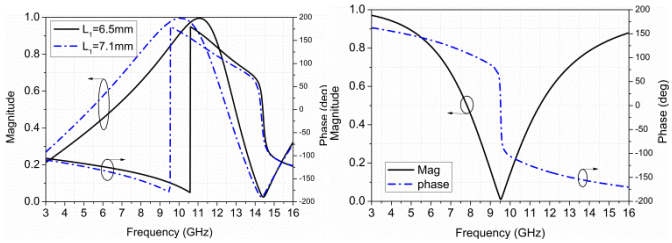

(a) (b)

Fig. 10. Reflection coefficient. (a) FSS1with different L_1. (b) FSS2.

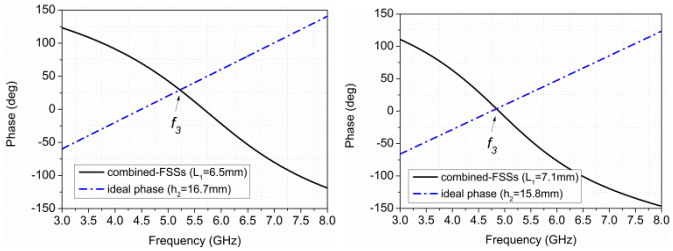

(a) (b)

Fig. 11. Reflection phase of the combined-FSSs. (a) $L_1 = 6.5$ mm. (b) $L_2 = 7.1$ mm.

can be easily adjusted by changing the cavity heights since they are determined by the two separated cavities. Fig. 9 shows the simulated directivity of the triband FPCA in X- and Ku-bands with different cavity heights. In this simulation, the dimensions of the FSS layers are 90×90 mm^2 in X-band and 70×70 mm^2 in Ku-band, respectively. It can be seen the peak directivity in Ku-band moves from 14.7 to 14.4 GHz when h_1 increases from 20.6 to 21 mm with remaining h_2. This value in X-band varies from 9.8 to 9.5 GHz with the increase of h_2 and unchanged of h_1.

It is desired to adjust f_3 with little impact on other two operating frequencies. Since f_3 is determined by the combined FSS layers, adjusting f_3 independently needs to consider the performance of the combined-FSSs. As can be seen in Fig. 10, tuning L_1 only increases the bandwidth of the bandpass without causing any frequency shift in Ku-band, which means f_1 and f_2 remain unchanged with the variation of L_1. Meanwhile, varying L_1 results in the property change of the combined-FSSs, which leads to some tuning of f_3. For example, according to Fig. 10(a), the calculated $h_2 = 16.7$ and 15.8 mm when L_1 is set as 6.5 and 7.1 mm, respectively. The calculated h_1 keeps as 21 mm since the FSS2 is unchanged. Due to the variation of the both L_1 and h_2, the reflection phase of the combined-FSSs is changed as well. Fig. 11 shows the reflection phase of this combined-FSSs under this two situation, where the f_3 can be adjusted to 4.8 and 5.3 GHz, respectively.

Fig. 12 shows the simulated directivity of this FPCA in three bands. It can be seen that the peak value of the directivity in C-band can

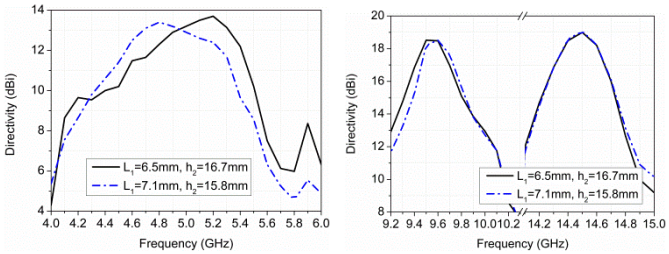

(a) (b)

Fig. 12. Directivity of the FPCA with different L_1 and h_2. (a) C-band. (b) X- and Ku-bands.

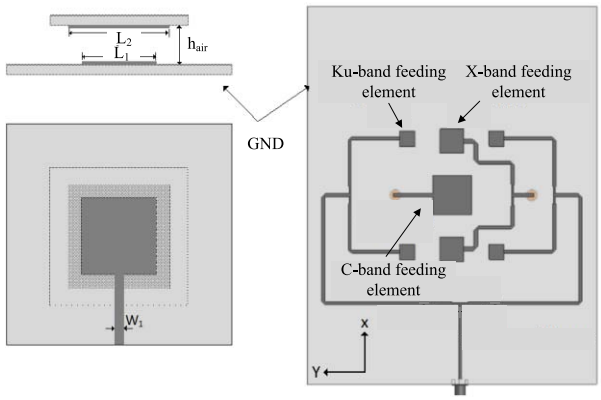

Fig. 13. Configuration of the feed unit and feed arrays.

be tuned via adjusting L_1 and h_2 with little impact on the directivity in X- and Ku-bands.

III. Triband High-Gain FPCA Design

A. Feed Antenna

The feed antenna consists of a C-band patch, 1×2 X-band sparse array and 2×2 Ku-band sparse array as shown in Fig. 13. The microstrip patch with the parasitic patch is employed as the element of the feed antennas. Rogers 4003C ($\varepsilon_r = 3.55$) with a thickness of 0.508 mm is chosen as the substrate. This patch is printed on the top side of the dielectric substrate of the ground plane. There is an air layer with the height of h_{air} between the driven patch and a parasitic patch. The dimensions of the feed units are determined by the operating frequencies. The designed parameters of the feed elements are $L_1 = 14.6$ mm, $L_2 = 16.3$ mm, $h_{\text{air}} = 4$ mm in C-band; $L_1 = 8.2$ mm, $L_2 = 9$ mm and $h_{\text{air}} = 2$ mm in X-band; $L_1 = 4.7$ mm, $L_2 = 5.7$ mm and $h_{\text{air}} = 1$ mm in Ku-band.

To make the feed antenna have a common center in C-, X-, and Ku-bands, the feed elements are carefully arranged. The C-band patch is placed in the center of the ground plane. Two X-band antennas are mounted on the right and left side of the C-band patch with the distance of 40 mm. Four Ku-band elements are around the C-band patch. The spacing between each element of the Ku-band feed array is 40 mm along the x-direction and 34 mm along the y-direction, respectively.

B. Computed and Measured Results of the Overall Design

The overall triband FPCA is calculated by the electromagnetic software CST MWS. The combined FSS layers consist of 13 units along the x-direction and 10 units along the y-direction, respectively, with the lateral size of 130×100 mm^2. This dimension is approximately $2.3\lambda \times 1.7\lambda$ at 5.2 GHz, $4.2\ \lambda \times 3.2\ \lambda$ at 9.6 GHz and $6.4\lambda \times 4.9\ \lambda$

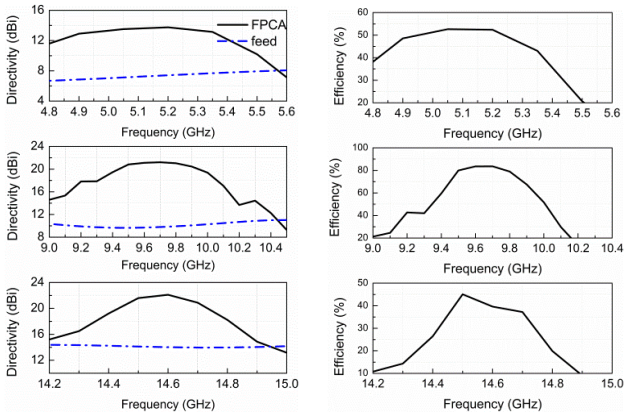

Fig. 14. (a) Simulated directivity. (b) Aperture efficiency.

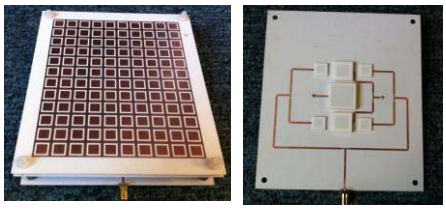

Fig. 15. Prototype of the proposed antenna.

at 14.6 GHz, respectively. The optimized parameters of the FSSs are $P = 10$ mm, $L_1 = 6.8$ mm, $L_2 = 3.6$ mm, $L_3 = 8.3$ mm, $S_1 = 0.5$ mm, $S_2 = 0.5$ mm, and $S_3 = 1.1$ mm. The feed antenna is placed at the center of the cavity with the optimized cavity heights of $h_1 = 20.5$ mm and $h_2 = 16.3$ mm, respectively. The computed directivity curves are shown in Fig. 14(a). The peak value happens at 5.2, 9.7, and 14.6 GHz, respectively, which reaches to 14.1, 21, and 22.2 dBi, respectively. Compared with the directivity of the feed antenna, the maximum increase of the directivity is 6.1, 11.4, and 7.2 dBi, respectively. The calculated aperture efficiency in each band is shown in Fig. 14(b). The maximum aperture efficiency in *C*- and *Ku*-bands is around 50%, and this value is more than 80% in *X*-band. Since the feed antenna is one patch in *C*-band, this results in insufficient illumination on the surface of the FSS layers, which leads to lower aperture efficiency. Although the *Ku*-band FPCA is fed by a 2×2 antenna array, the electrical dimension of the FSS layers is too large, which leads to lower aperture efficiency as well. Thus, when we design the triband FPCA, we should consider the tradeoff between the performance of each band.

The prototype is fabricated as shown in Fig. 15. The overall profile of this antenna is 21 mm, which is approximately 0.36 λ at 5.2 GHz. Fig. 16(a) shows the calculated and measured S-parameters of the proposed antenna. It can be found that this antenna works well in *C*-, *X*-, and *Ku*-bands as expected. The measured S_{11} below -10 dB is from 5.1 to 5.5 GHz, 9.6 to 10.2 GHz, and 14.4 to 16.0 GHz with the impedance bandwidth of 7.5%, 6.1%, and 10.5%, respectively. Some small differences between the simulated and measured results are mainly due to the inaccuracies during the antenna fabrication and assembly. The realized gain of this prototype is shown in Fig. 16(b). There is a good agreement between the measured results and the estimated value, where the measured peak gain occurs at 5.2, 9.7, and 14.6 GHz, reaching 13.4, 19.7, and 20 dBi, respectively.

The measured and simulated radiation patterns at 5.2, 9.6, and 14.6 GHz are shown in Fig. 17. The measured results have good agreements with the computed radiation patterns. It can be seen that the peak radiation occurs in the broadside direction at these

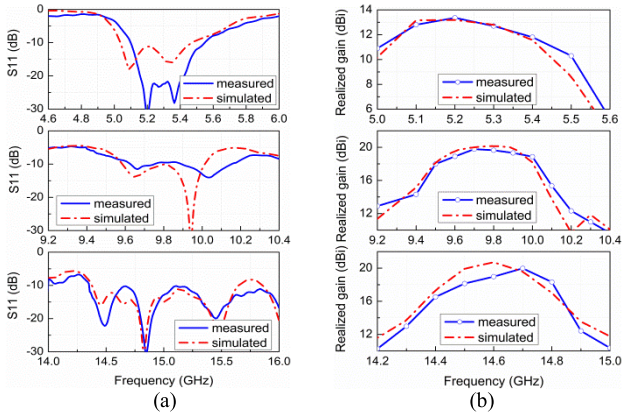

Fig. 16. (a) Measured S-parameters. (b) Measured realized gain.

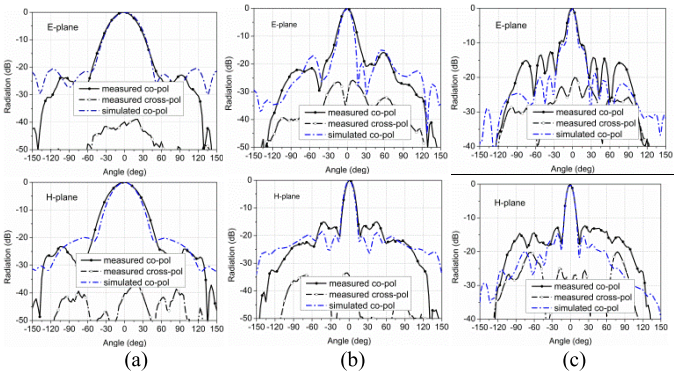

Fig. 17. Measured and simulated radiation patterns. (a) 5.2 GHz. (b) 9.6 GHz. (c) 14.6 GHz.

three frequencies, and sidelobe lower than -15 dB is obtained in the whole operating frequency band. Moreover, cross polarization better than 35 dB in broadside is obtained as well.

IV. Conclusion

A technique of designing a triband low-profile high-gain FPCA with two FSS layers is proposed in this communication. The study of tuning frequency in each band and the achievable frequency range of this proposed antenna are present. The operating frequencies can be adjusted independently within its achievable frequency ratio. To the design concept, a high gain triband FPCA operating in *C*-/*X*-/*Ku*-bands is designed, fabricated and measured. The profile of this proposed antenna is 0.36 wavelength at its lowest frequency, with the frequency ratio of 2.8:1.52:1. The prototype gives measured peak gain of 13.4, 19.7, and 20 dBi at 5.2, 9.7, and 14.6 GHz, respectively, with good impedance matching. This proposed antenna has a promising performance such as triband, high gain, low profile, simple feed network, easy fabrication, and low cost.

References

[1] W. A. Imbriale, S. Gao, and L. Boccia, Eds., *Space Antenna Handbook*. London, U.K.: Wiley, May 2012.

[2] Q. Luo *et al.*, "Design and analysis of a reflectarray using slot antenna elements for Ka-band SatCom," *IEEE Trans. Antennas Propag.*, vol. 63, no. 4, pp. 1365–1374, Apr. 2015.

[3] N. A. Aboserwal, C. A. Balanis, and C. R. Birtcher, "Conical horn: Gain and amplitude patterns," *IEEE Trans. Antennas Propag.*, vol. 61, no. 7, pp. 3427–3433, Jul. 2013.

[4] O. Yurduseven, D. Cavallo, A. Neto, G. Carluccio, and M. Albani, "Parametric analysis of extended hemispherical dielectric lenses fed by a broadband connected array of leaky-wave slots," *IET Microw., Antennas Propag.*, vol. 9, no. 7, pp. 611–617, May 2014.

[5] S. Ye, J. Geng, X. Liang, Y. J. Guo, and R. Jin, "A compact dual-band orthogonal circularly polarized antenna array with disparate elements," *IEEE Trans. Antennas Propag.*, vol. 63, no. 4, pp. 1359–1364, Apr. 2015.

[6] D. M. Pozar and S. D. Targonski, "A shared-aperture dual-band dual-polarized microstrip array," *IEEE Trans. Antennas Propag.*, vol. 49, no. 2, pp. 150–157, Feb. 2001.

[7] G. Vetharatnam, C. B. Kuan, and C. H. Teik, "Combined feed network for a shared-aperture dual-band dual-polarized array," *IEEE Antennas Wireless Propag. Lett.*, vol. 4, pp. 297–299, 2005.

[8] G. V. Trentini, "Partially reflecting sheet arrays," *IRE Trans. Antennas Propag.*, vol. 4, no. 4, pp. 666–671, Oct. 1956.

[9] A. Pirhadi, M. Hakkak, F. Keshmiri, and R. K. Baee, "Design of compact dual band high directive electromagnetic bandgap (EBG) resonator antenna using artificial magnetic conductor," *IEEE Trans. Antennas Propag.*, vol. 55, no. 6, pp. 1682–1690, Jun. 2007.

[10] Y. Ge, K. P. Esselle, and T. S. Bird, "A method to design dual-band, high-directivity EBG resonator antennas using single-resonant, single-layer partially reflective surfaces," *Prog. Electromagn. Res. C*, vol. 13, pp. 245–257, 2010.

[11] B. A. Zeb, Y. Ge, K. P. Esselle, Z. Sun, and M. E. Tobar, "A simple dual-band electromagnetic band gap resonator antenna based on inverted reflection phase gradient," *IEEE Trans. Antennas Propag.*, vol. 60, no. 10, pp. 4522–4529, Oct. 2012.

[12] F. Meng and S. K. Sharma, "A dual-band high-gain resonant cavity antenna with a single layer superstrate," *IEEE Trans. Antennas Propag.*, vol. 63, no. 5, pp. 2320–2325, May 2015.

[13] H. Moghadas, M. Daneshmand, and P. Mousavi, "A dual-band high-gain resonant cavity antenna with orthogonal polarizations," *IEEE Antennas Wireless Propag. Lett.*, vol. 10, pp. 1220–1223, 2011.

[14] H. Moghadas, M. Daneshmand, and P. Mousavi, "Single-layer partially reflective surface for an orthogonally-polarised dual-band high-gain resonant cavity antenna," *IET Microw., Antennas Propag.*, vol. 7, no. 8, pp. 656–662, Jun. 2013.

[15] Y. Ge and C. Wang, "A tri-band Fabry–Perot cavity for antenna gain enhancement," in *Proc. IEEE Antennas Propag. Soc. Int. Symp. (APSURSI)*, Jul. 2013, pp. 284–285.

[16] A. Ghasemi, S. N. Burokur, A. Dhouibi, and A. de Lustrac, "High beam steering in Fabry–Pérot leaky-wave antennas," *IEEE Antennas Wireless Propag. Lett.*, vol. 12, pp. 261–264, 2013.